Predissociation dynamics of the HCl–$(H_2O)_3$ tetramer: An experimental and theoretical investigation

Kristen Zuraski, Qingfeng (Kee) Wang, Daniel Kwasniewski, Joel M. Bowman, and Hanna Reisler

Citation: The Journal of Chemical Physics **148**, 204303 (2018); doi: 10.1063/1.5026585
View online: https://doi.org/10.1063/1.5026585
View Table of Contents: http://aip.scitation.org/toc/jcp/148/20
Published by the American Institute of Physics

Predissociation dynamics of the HCl–$(H_2O)_3$ tetramer: An experimental and theoretical investigation

Kristen Zuraski,[1] Qingfeng (Kee) Wang,[2] Daniel Kwasniewski,[1] Joel M. Bowman,[2,a)] and Hanna Reisler[1,a)]

[1]*Department of Chemistry, University of Southern California, Los Angeles, California 90089-0482, USA*
[2]*Department of Chemistry and Cherry L. Emerson Center for Scientific Computation, Emory University, Atlanta, Georgia 30322, USA*

(Received 21 February 2018; accepted 11 May 2018; published online 29 May 2018)

The cyclic HCl–$(H_2O)_3$ tetramer is the largest observed neutral HCl–$(H_2O)_n$ cluster. The vibrational predissociation of HCl–$(H_2O)_3$ is investigated by theory, quasiclassical trajectory (QCT) calculations, and experiment, following the infrared excitation of the hydrogen-bonded OH-stretch fundamental. The energetically possible dissociation pathways are HCl + $(H_2O)_3$ (Pathway 1) and H_2O + HCl–$(H_2O)_2$ (Pathway 2). The HCl and H_2O monomer fragments are observed by 2 + 1 resonance enhanced multiphoton ionization combined with time-of-flight mass spectrometry, and their rotational energy distributions are inferred and compared to the theoretical results. Velocity map images of the monomer fragments in selected rotational levels are used for each pathway to obtain pair-correlated speed distributions. The fragment speed distributions obtained by experiment and QCT calculations are broad and structureless, encompassing the entire range of allowed speeds for each pathway. Bond dissociation energies, D_0, are estimated experimentally from the endpoints of the speed distributions: 2100 ± 300 cm^{-1} and 2400 ± 100 cm^{-1} for Pathway 1 and Pathway 2, respectively. These values are lower but in the same order as the corresponding calculated D_0: 2426 ± 23 cm^{-1} and 2826 ± 19 cm^{-1}. The differences are attributed to contributions from vibrational hot bands of the clusters that appear in the high-speed tails of the experimental pair-correlated distributions. Satisfactory agreement between theory and experiment is achieved when comparing the monomer fragments' rotational energies, the shapes of the speed distributions, and the average fragment speeds and center-of-mass translational energies. Insights into the dissociation mechanism and lifetime are gained from QCT calculations performed on a previously reported many-body potential energy surface. It is concluded that the dissociation lifetime is on the order of 10 ps and that the final trimer products are in their lowest energy cyclic forms. *Published by AIP Publishing.* https://doi.org/10.1063/1.5026585

I. INTRODUCTION

Water-hydracid complexes are prototype systems for the study of hydrogen bond (H-bond) properties and the mechanisms of acid solvation. The unique properties of water arise from its ability to form H-bonds, which often leads to the stabilization of intermediates, the shifting of molecular vibrational energies, and the lowering of activation barriers for reactions.[1,2] The ability of water to stabilize ions is also well known;[3] however, a detailed understanding of the dynamics leading to acid ionization within mixed clusters is uncertain. A bottom-up approach aims to identify trends in H-bonds' dissociation through isolation of small mixed clusters. This starts with dimers containing one water and one hydrogen halide species and then sequentially adding solvent water molecules to compare properties of larger cyclic networks.

The present work focuses on the vibrational predissociation (VP) of the HCl–$(H_2O)_3$ tetramer (referred to henceforth as HWWW), the largest HCl–$(H_2O)_n$ cluster observed without ionization to solvated $H_3O^+ + Cl^-$. Addition of one or two water molecules to this mixed cluster is expected to initiate proton migration to generate a stable solvent ion pair.[4–11] Although the existence and structure of HWWW was debated in the past, the most recent calculations confirm that it is stable and its optimized geometry is cyclic, as shown in Fig. 1.[4,12–15]

An investigation of this mixed cluster is also interesting because there are two close-lying dissociation channels that can be accessed by excitation of the intramolecular OH-stretch fundamentals, yielding HCl (Pathway 1) and H_2O (Pathway 2) monomer fragments,

$$\text{HCl–}(H_2O)_3 \rightarrow \text{HCl} + (H_2O)_3, \quad (1)$$

$$\text{HCl–}(H_2O)_3 \rightarrow H_2O + \text{HCl–}(H_2O)_2. \quad (2)$$

An open question is whether the final trimer products, $(H_2O)_3$ and HCl–$(H_2O)_2$, have cyclic or open-chain configurations. The cyclic forms of these trimers are more stable energetically; however, the transition states required for their formation via VP of the tetramer are tight and thus disfavored by entropy. The theoretical/experimental examination presented here strives to answer this intriguing question.

a)Authors to whom correspondence should be addressed: reisler@usc.edu and jmbowma@emory.edu

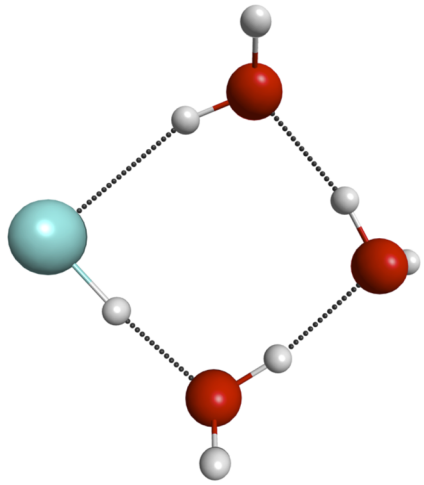

FIG. 1. The global minimum configuration of HCl–$(H_2O)_3$.

The investigation of the VP of HWWW poses challenges for both experiment and theory. In experiments, separating the infrared (IR) transition of the H-bonded OH stretch of the desired tetramer from transitions of other $(HCl)_m$–$(H_2O)_n$ clusters was key. In recent spectroscopic assignments in He droplets,[16] the H-bonded OH stretch vibrations of several pure water and mixed HCl-water clusters were identified. In spite of the close proximity of transitions in several clusters, HWWW has IR bands that are isolated. In supersonic molecular beams, however, these bands are broader and partially overlap. In our previous experimental work, we presented arguments that the broad band at 3530–3550 cm^{-1} is associated with H-bonded OH stretch vibrations of HWWW and we identified H_2O monomers as VP products.[17] From the highest translational energy release in the VP of HWWW, we inferred that the dissociation energy (D_0) for Pathway 2 was 2400 ± 100 cm^{-1}.[17]

Theoretical studies of the VP dynamics of HWWW are also challenging, requiring an accurate potential energy surface (PES) that describes the complex at the high energies of dissociation to the two product channels of interest here. (The need to run thousands of trajectories for roughly 10 ps rules out an *ab initio* direct dynamics approach.) Here the PES employed is based on high-level *ab initio* many-body components, as described in detail and tested previously by Mancini and Bowman.[14] Structures were optimized and vibrational frequencies were determined using different approximations, which confirmed the vibrational assignments of the experimentally observed IR spectra of mixed clusters. Previous calculations for dimers and trimers gave H-bond dissociation energies that were in close agreement with experiments. These studies are summarized in recent papers and review articles.[1,18–22] In addition, quasiclassical trajectory (QCT) calculations performed on these highly accurate PESs were used successfully before to determine the VP dynamics and dissociation energies of $(H_2O)_2$, HCl–H_2O, $(H_2O)_3$, and $(HCl)_3$.[1,18,20–22]

In this paper, we present the results of a joint experimental and theoretical study of the predissociation of HWWW via Pathways 1 and 2. In addition to being the first tetramer species to be investigated in detail, it is also the first mixed HCl-water VP dynamics study for a system larger than dimers. We report our best experimental and theoretical estimates for the dissociation energies for Pathways 1 and 2, rotational energy distributions for the HCl and H_2O monomer fragments, and fragment speed distributions, following excitation of the H-bonded OH stretch. Moreover, we gain deeper insight into the predissociation dynamics by analyzing dissociative trajectories, obtained by QCT calculations, for the two dissociation pathways. These indicate that cyclic trimer fragments are formed in the two pathways, and the dissociation mechanism follows trends congruent with smaller neutral clusters.

II. EXPERIMENTAL METHODS

The experimental procedures used in this work are similar to those used in the previous study of Pathway 2;[17] therefore, only aspects relevant to Pathway 1 are described in detail. For Pathway 1, mixtures of 0.6% H_2O and 2% HCl (99.995%) in ~2-atm helium (99.999%) were prepared and introduced through a 0.5 mm orifice of a pulsed piezoelectric valve (~200 μs opening time, 10 Hz repetition rate) into a differentially pumped chamber (~3.0×10^{-8} Torr base pressure; ~1.2×10^{-5} Torr working source pressure).

Focused IR laser radiation [optical parametric oscillator/amplifier (OPO/OPA) system, ~3.0 mJ/pulse; 20 cm focal length (f.l.) lens, 0.4 cm^{-1} bandwidth] was used to excite the H-bonded OH stretch fundamental of the cluster at 3550 cm^{-1}, and focused ultraviolet radiation (Continuum ND6000, 235–250 nm, ~0.18 mJ/pulse; 20 cm f.l. lens) was used to probe the HCl fragments in selected rotational states via 2 + 1 resonance enhanced multiphoton ionization (REMPI). "IR On" signals were collected, while exciting the OH stretch of the tetramer, whereas "IR Off" signals corresponded to an off-peak 3652 cm^{-1} position, where signals from other $(HCl)_n$–$(H_2O)_m$ clusters were at a minimum. This takes into account background signals from both monomers in the beam and monomer fragments from other clusters. For each pathway, the laser conditions (timing, focusing, and power) were optimized to enhance the signal from HWWW, while minimizing signals from other clusters. The IR wavelength was calibrated using ammonia in a photoacoustic cell, and the ultraviolet radiation was calibrated using known 2 + 1 REMPI transitions of HCl and H_2O.[23,24]

Experiments were run using two different data acquisition modes: (1) time-of-flight mass spectrometry (TOF-MS) for recording IR action spectra, 2 + 1 REMPI spectra, and optimizing the timings and alignment of the instrument, and (2) velocity map imaging (VMI) for deriving pair-correlated rovibrational distributions of the cofragments by monitoring specific rotational levels of the HCl or H_2O monomer fragments. Raw images were converted to fragment speed distributions in pixel space using the BASEX method,[25] and the speed distributions were converted to center-of-mass (c.m.) translational energy distributions using the appropriate Jacobian and momentum conservation.[26]

Using the TOF-MS mode, scans were taken across the 2 + 1 REMPI transitions of HCl to determine the relative populations of individual rotational states and to set an upper limit

for the dissociation energy of Pathway 1. To encompass the full range of all the energetically possible rotational levels of HCl, transitions through the following intermediate states were used: $f^3\Delta_2$ ($v' = 0$) for $J'' = 3$–6, $F^1\Delta_2$ ($v' = 0$) for $J'' = 5$–8, and $V^1\Sigma^+$ ($v' = 11$ and 12) for $J'' = 5$–11.[22,27,28] The spectra were analyzed by comparison to PGOPHER[29] simulations generated with constants from Green *et al.*[23] While scanning across these transitions, "IR On" and "IR Off" signals were collected intermittently at each wavelength position. REMPI peaks were fit with a Gaussian function and integrated. The difference between the "IR On" and "IR Off" values was then used to infer relative HCl fragment populations after correction by appropriate calibration constants, which take into account predissociation in the upper electronic states (see the supplementary material for details).[27,28] Population distributions of the HCl monomer fragments obtained via different intermediate states were normalized to each other using $J'' = 5$, which was accessed by all three transitions.

For Pathway 2, H_2O transitions via the $\tilde{C}^1B_1(000) \leftarrow \tilde{X}^1A_1(000)$ intermediate state were used, and the 2 + 1 REMPI spectra were compared to simulations using PGOPHER with spectroscopic data from Yang *et al.*[17,24,29] In this case, it was not feasible to infer rotational state populations due to spectral congestion and the complexity of the REMPI spectra. Instead, temperatures of the water monomers and fragments were estimated by comparison to a PGOPHER simulation that includes experimentally determined predissociation lifetimes of rotational levels in the $\tilde{C}^1B_1(000)$ state.[17,24] Background signals from water monomers coming from the molecular beam were estimated from REMPI scans obtained under "IR off" conditions. The difference between the "IR On" and "IR Off" spectra gave the signals from the monomer fragments.

The temperatures of the clusters in the beam were estimated from the temperatures of the monomers under the conditions optimized for the VP studies of each pathway. They were 15 ± 5 K and 44 ± 10 K for H_2O and HCl monomers, respectively, determined at the crossing point of the molecular and laser beams at the interaction region (see the supplementary material for details).

III. THEORETICAL METHODS AND ENERGETICS

As noted above, the PES used was a highly accurate many-body potential constructed by Mancini and Bowman.[14] Accurate dissociation energies for numerous dissociation pathways, including the high energy breakup to H + W + W + W, were calculated using D_e values from complete basis set (CBS) calculations and zero-point energies (ZPEs) using an unbiased diffusion Monte Carlo (DMC) method for HWWW and various product fragments. (The results and details are given in the supplementary material.) The results of relevance here are as follows: D_e values are 3008 and 3634 cm^{-1} for Pathways 1 and 2, respectively, and the corresponding D_0 values are 2426 ± 23 and 2826 ± 19 cm^{-1}, respectively. In Sec. IV, we compare these values to the experimental results.

The VP dynamics reported here are based on QCT calculations very similar to those reported previously,[1,18] so we only describe them briefly. Trajectories were initiated at the global minimum configuration of HWWW, which is depicted in Fig. 1. The standard harmonic normal mode sampling was done for initial conditions in which all modes except the mode excited are sampled from the zero-point state. The harmonic frequencies are given in Table S1 of the supplementary material. Two H-bonded OH stretch modes were considered for this excitation. One is mode 24 and the other is mode 22; these are depicted in Fig. S1 of the supplementary material. Mode 24 has a harmonic frequency of 3749 cm^{-1} and a previous[14] approximate anharmonic treatment of this mode reported a fundamental energy of 3547 cm^{-1} which is close to the experimental excitation energy (3550 cm^{-1}). So this mode is the likely candidate for the mode excited experimentally. However, calculations were also done with mode 22 excited, which permits an examination of possible mode-specific effects in the dissociation. After transformation from normal coordinates and momenta to Cartesian coordinates and momenta, the energy is not the harmonic value because the actual potential is anharmonic and, in addition, the total angular momentum is not exactly zero. A standard procedure to adjust the Cartesian momenta is done to eliminate angular momentum and also to bring the total energy to a desired value. Since we know the rigorous anharmonic ZPE from DMC calculations (17 683 cm^{-1}) and the experimental excitation energy (3550 cm^{-1}), the total energy is the sum of these two, i.e., 21 233 cm^{-1}. Trajectories were propagated using a velocity-Verlet algorithm with a step size of 0.06 fs and terminated when any individual bond length exceeded 16 Å.

Final product channels were categorized by the distance between the monomers. Thus, distances between all possible fragments were monitored and the products of a dissociated trajectory were identified based on the condition that the shortest intermolecular distance between one monomer and other fragments was greater than 6.5 Å. The HWWW complex dissociates classically into numerous products, of which only Pathways 1 and 2 are rigorously open when considering ZPE of the fragments (Table S2 in the supplementary material). Thus analysis is done only for the set of trajectories giving these two channels.

A total of roughly 60 000 trajectories were run, of which 30% dissociated to Pathway 1 and 40% to Pathway 2, for excitation of either mode 22 or mode 24, without consideration of either fragments' ZPE. Other channels account for the remaining 30% of the total trajectories and were excluded from analysis. We return to this branching ratio and its dependence on the treatment of ZPE of the fragments in Sec. IV. However, we note that the equality of the branching ratio for excitation of either mode 22 or 24 already indicates statistical dynamics. Also, note that the dissociation time for both channels was approximately 8 ps.

The analysis of the fragments' internal energies was done in the standard way, with subsequent comparison to the experiments in mind. Specifically, for each trajectory corresponding to Pathway 1, the magnitude of the classical angular momentum of HCl (in atomic units), j, was obtained. From this, the quantum number J was obtained from $j^2 = J(J+1)$ and rounded to the nearest integer. For Pathway 2, the rotational and vibrational energies of the H_2O product were determined

as follows. First, the total classical rovibrational energy of H_2O was determined. Then, using the same method to prepare initial conditions with zero total angular momentum, the angular momentum of H_2O was removed and subsequently the total internal energy was determined. This is by definition the vibrational energy of H_2O, and the difference with the total rovibrational energy is the classical rotational energy. In this way, the vibrational and rotational energies of the fragments were obtained. The c.m. translational energy, E_t, was calculated directly using $E_t = 0.5\mu v^2$, where μ is the reduced mass of the two fragments and v is the relative speed. In the experiments, E_t was calculated from the measured fragment speed as described in Sec. II. Standard histogram binning was done for the HCl rotational distribution. For the H_2O fragments, selected $J_{Ka,Kc}$ levels were observed in the experiments. In principle, J, K_a, and K_c can be determined classically and then binned. However, the number of trajectories needed to obtain a statistically significant result would require a prohibitive amount of computer time. Thus, in the QCT calculations, only the classical rotational and vibrational energy of H_2O was determined.

As noted above, most of the fragments were formed with energy less than the ZPE. Thus several standard constraints were applied by comparing the calculated vibrational energy to the DMC-calculated ZPE of the fragments. The "soft ZPE constraint" requires $E_{vib}(HCl–(H_2O)_2) + E_{vib}(H_2O) > ZPE(HCl–(H_2O)_2) + ZPE(H_2O)$ in Pathway 2 and $E_{vib}((H_2O)_3) + E_{vib}(HCl) > ZPE((H_2O)_3) + ZPE(HCl)$ in Pathway 1, while the "hard ZPE constraint" requires each fragment to have a vibrational energy greater than the ZPE of the fragment. Finally, we consider a "hard ZPE on monomer" which requires only the dissociated water or HCl to satisfy the ZPE condition. Ideally, the hard ZPE constraint should be applied; however, this results in the rejection of a very large number of trajectories, which leads to final results (such as rotational distributions) that are statistically highly uncertain.

IV. RESULTS AND DISCUSSION

A. Fragment speed distributions

Experimental speed distributions of the monomer fragments were obtained by reconstruction of velocity mapped raw images obtained by 2 + 1 REMPI detection of either HCl or H_2O in selected rotational levels. Pixels on the detector were converted to speeds using calibration factors obtained by comparison with previously published speed distributions.[17,19] Due to the high density of internal states in the trimer cofragments, the speed distributions displayed no clear structural features and appeared statistical-like (see below). In this case, only the endpoints of the distributions could be used to estimate the dissociation energy. This is in contrast to small dimers, such as HCl–H_2O, where distinct structures correlated with rotational states of the cofragment were exploited to obtain precise D_0 values.[18,19] Nevertheless, the endpoints of the speed distributions were reproducible, allowing us to estimate the dissociation energies for each pathway. The endpoints were clearer for Pathway 2 due to much higher signal/noise ratios.

Figure 2 shows the speed distributions of the HCl and H_2O monomer fragments monitored in the indicated rotational states. Distributions for Pathway 2 were reported before as a function of center-of-mass (c.m.) translational energy.[17] Note that in the previously reported distributions, no Jacobian was used in converting intensities when transforming fragment speed to c.m. translational energy distributions, but this omission did not affect the highest value of the translational energy.

The shaded areas in Fig. 2 depict our estimates for the ranges of acceptable endpoints in each distribution. From the

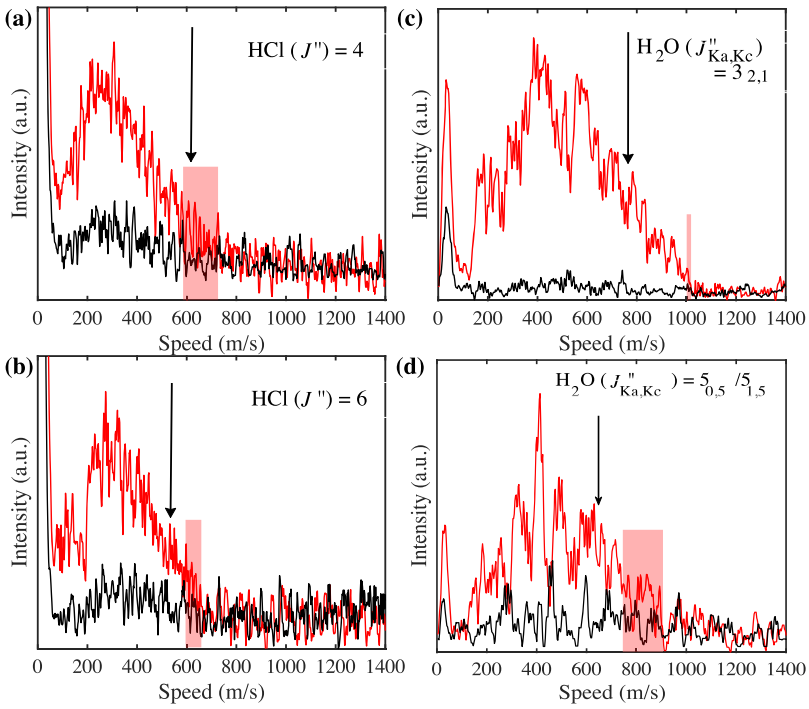

FIG. 2. Speed distributions obtained by monitoring (a) $J'' = 4$ and (b) $J'' = 6$ of the HCl monomer fragments following the dissociation pathway HWWW → H + WWW, and (c) $J''_{Ka,Kc} = 3_{2,1}$ and (d) $J''_{Ka,Kc} = 5_{0,5}/5_{1,5}$ of the H_2O fragments from the HWWW → W + HWW pathway. Red and black plots are obtained using "IR On" and "IR Off" conditions, respectively. Shaded regions indicate uncertainty in determining the endpoints of the experimental distributions. Arrows indicate the location of endpoints for the speed distributions expected from the calculated dissociation energies.

ranges for the HCl $J'' = 4$ and 6 speed distributions, we estimate the D_0 for Pathway 1 to be 2100 ± 300 cm^{-1}. Having a much higher signal/noise ratio, the corresponding ranges for Pathway 2 are smaller, resulting in D_0 = 2400 ± 100 cm^{-1}, as described before.[17] As noted above, the calculated dissociation energies are 2426 ± 23 cm^{-1} and 2826 ± 19 cm^{-1} for Pathways 1 and 2, respectively. These values correspond to the cyclic forms of the trimer products (see below). The fragment speeds corresponding to the calculated D_0 values are indicated by arrows in Fig. 2.

Experimentally, there are two problems in determining D_0 from the highest speed. First, as described above, assigning the endpoints of the distributions has inherent uncertainty because of the low signal/noise in the tail region; therefore, for Pathway 1, only ranges of acceptable values can be determined. Second, when the parent cluster has a significant internal energy, especially in the form of vibrational energy, the highest translational energy may be correlated with hot bands, in which case the experimentally determined dissociation energy is only a lower limit to D_0 of the cold tetramer, as discussed below.

Following conversion of fragment speeds to c.m. translational energy distributions, D_0 was obtained by using conservation of energy,

$$E_{int}(v,r) + E_{IR} = D_0 + E_r(\text{monomer}) + E_{v,r}(\text{confragment}) + E_t, \quad (3)$$

where $E_{int}(v,r)$ is the internal rovibrational energy of the HWWW parent cluster, E_{IR} is the energy imparted by IR excitation, E_r(monomer) is the (known) energy of the monitored HCl or H_2O rotational levels, and $E_{v,r}$ (cofragment) is the rovibrational energy of the cofragment which is zero when the c.m. translational energy (E_t) release reaches the maximum value allowed by energy conservation. The greatest difficulty is in assessing $E_{int}(v,r)$. The average rotational energy of the cluster is estimated from the rotational temperatures of the monomers: 30 ± 15 cm^{-1} and 10 ± 5 cm^{-1} for HCl and H_2O, respectively. However, it is impossible to assess accurately the vibrational energy of the clusters because the low-energy intermolecular vibrations may not be cooled efficiently in the supersonic expansion.

Additional insight can be gained by comparing the experimental pair-correlated speed distributions to the ones calculated by QCT. The speed distributions calculated for HCl $J'' = 4$ and 6 rotational levels (Pathway 1) are shown in Fig. 3 for excitation of mode 22 [panels (a) and (b)] and for excitation of mode 24 [panels (c) and (d)]. The QCT distributions were obtained by using soft ZPE constraints. This constraint was chosen as the best compromise between accuracy and the number of trajectories (see Fig. S2 and Table S3 in the supplementary material). Clearly the experimental and calculated peaks of the distributions appear similar, and the QCT results for mode 22 and mode 24 are virtually identical. In addition to comparing the peak positions of the speed distributions, we also compared the average fragment speeds and average c.m. translational energies, and the comparisons are summarized in Table I. As seen in Fig. 3 and Table I, the theoretical calculations and experimental distributions have similar peak positions, shapes, and average speeds, but the experimental distributions include low-intensity tails that extend to higher speeds leading to the disagreement in the D_0 values. The calculated D_0 values are higher for both pathways than those observed experimentally, but in both cases Pathway 1 (HCl fission) has the lower energy. As noted already,

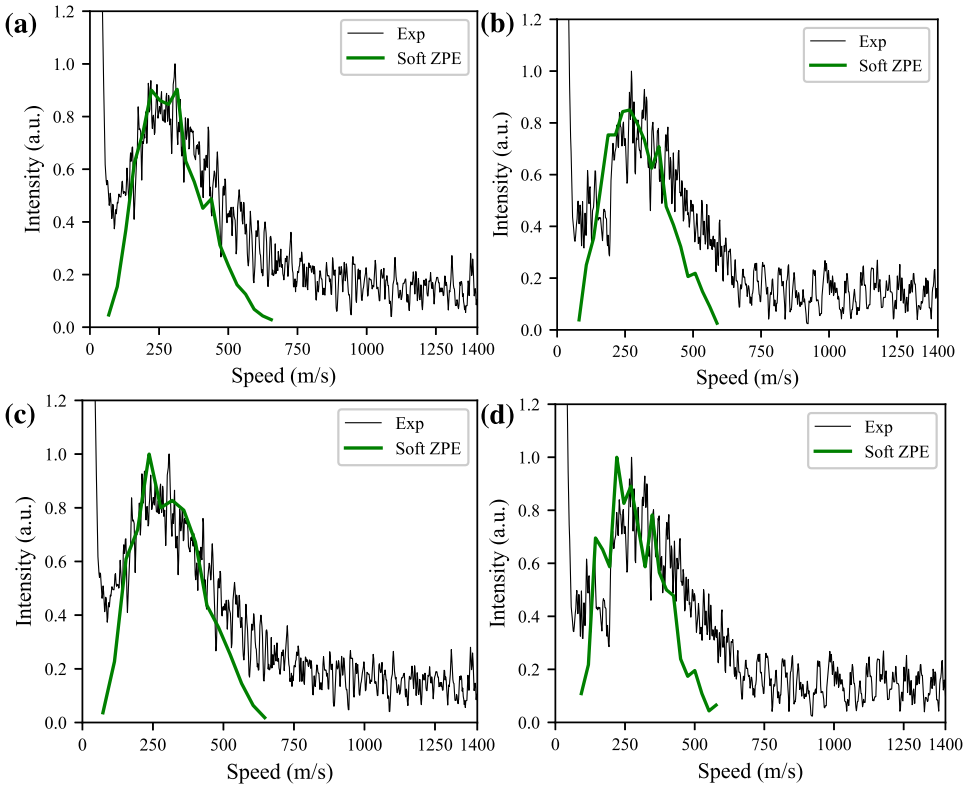

FIG. 3. Experimental and theoretical (using soft ZPE constraints) speed distributions for HCl monomer fragments in rotational levels $J'' = 4$ [(a) and (c)] and $J'' = 6$ [(b) and (d)]. QCT speed distributions for excitation of mode 22 [(a) and (b)] and mode 24 [(c) and (d)] are shown. The large intensity at the origin of the experimental data is the result of monomers in the molecular beam.

TABLE I. Experimental and theoretical values (soft ZPE) for approximate peak positions, the average speed of the HCl fragment, and the average translational energy E_t.

HCl rotation	$J'' = 4$		$J'' = 6$	
	Experimental	Theoretical	Experimental	Theoretical
Peak position (m/s)	270	306,[a] 252[b]	290	261,[a] 271[b]
Average speed (m/s)	329	303,[a] 312[b]	324	297,[a] 287[b]
Average E_t (cm^{-1})	273	264,[a] 278[b]	264	250,[a] 232[b]

[a]Obtained by exciting mode 22.
[b]Obtained by exciting mode 24.

corresponding QCT calculations for specific $J''_{Ka,Kc}$ levels of the water fragment (Pathway 2) could not be done due to an insufficient number of trajectories for specific rotational levels.

The similarity of the results for the two investigated modes and the statistical-like appearance of the speed distributions are not surprising, given the large density of states of the reactants and products. We calculated a lower limit for the density of states of the excited parent and fragment clusters by using the Beyer-Swinehart algorithm[30,31] for direct count of harmonic vibrational states. The vibrational density of states of the tetramer, obtained using the harmonic frequencies listed in the supplementary material, is approximately 1×10^6 /cm^{-1} at 3500 cm^{-1}. The corresponding values for the water trimer products, obtained using the calculated intermolecular frequencies listed in Table 7 of Ref. 32, range from 5 to 20 /cm^{-1} for the 500–1000 cm^{-1} available energies of this work.

Previous comparisons of theory and experiment for D_0 values of small H-bonded clusters, such as $(H_2O)_2$, $(HCl)_3$, and H_2O–HCl, showed excellent agreement.[1,18–20,22] In these cases, the experimental D_0 values were obtained by exploiting distinct structural features in each distribution, rather than using the endpoints. As mentioned above, a plausible explanation for the present disagreement is the participation of hot bands captured by IR excitation at 3550 cm^{-1}, which results in fragments with higher maximum speeds. In this case, the parent cluster would have excess internal energy, $E_{int}(v,r)$, which is not taken into account properly in determining D_0. The possible participation of hot bands is also supported by the observed large width (about 25 cm^{-1} full width) of the H-bonded OH stretch transition being excited,[17] which may include contributions from hot bands. This band lies in the proximity of transitions of other clusters (Ref. 17 and its supplementary material), and from a spectroscopic perspective, the 3550 cm^{-1} excitation energy within the broad band was chosen because of its isolation from other mixed-clusters' transitions.[16] According to calculations, there are 11 low-energy intermolecular vibrations in the tetramer parent within 400 cm^{-1} of the ground vibrational state, which makes the contribution of hot bands a likely explanation for the difference between theory and experiment (see Table S1 in the supplementary material). However, because the majority of the fragments' signals derive from cold clusters, we expect the average speeds and peak positions to give a better match to the theoretical results than D_0, as is indeed the case. Fragments from hot clusters would be manifested mainly in the low-intensity tails of the speed distributions. Hot band transitions of clusters have been observed before under our experimental expansion conditions, but not in lower temperature studies, such as in He droplets.[33]

B. Fragment rotational energy distributions

The rotational energy distribution of the HCl fragments following Pathway 1 was determined by both theory and experiment. Figure 4 shows examples of the 2 + 1 REMPI spectra (after background subtraction) obtained via the $f^3\Delta_2 - X^1\Sigma^+$ (0,0) and $F^1\Delta_2 - X^1\Sigma^+$ (0,0) intermediate transitions. An upper limit of $D_0 \leq 2830$ cm^{-1} is obtained for Pathway 1 from $J'' = 8$, the highest HCl rotational level that could be observed with confidence. Populations in $J'' = 0$–2 could not be obtained because of large background from HCl monomers. Figure 5 shows the relative rotational state populations plotted as a function of rotational energy along with calculated rotational energy distributions. The QCT derived distributions for excitation of modes 22 and 24 (both with 3550 cm^{-1} excitation) show the same general trend as the experiment but decrease more slowly with increasing energy. The hard and soft ZPE constraints show that the rotational energy cutoffs correspond to $J'' = 8$ and $J'' = 10$, respectively, in the HCl monomer fragment. There are multiple explanations for the discrepancy between theory and experiment, including the known difficulty in interpreting quantum rotations using classical calculations

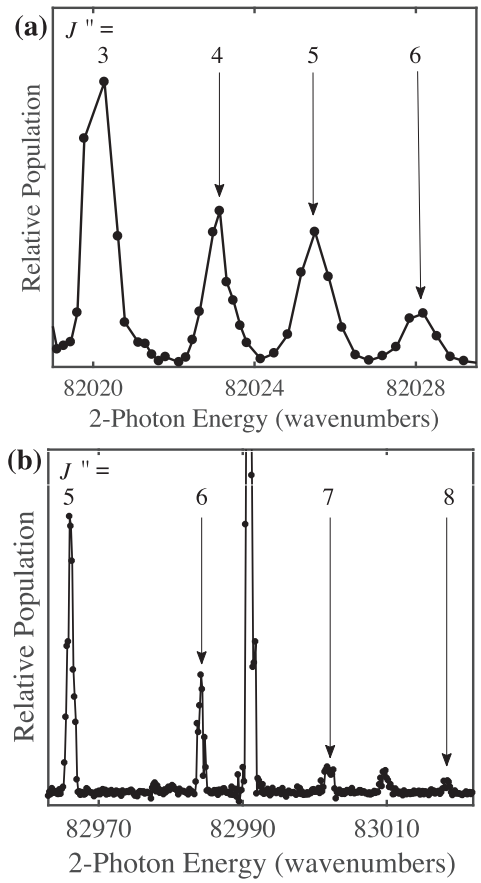

FIG. 4. (2 + 1) REMPI spectra of $H^{35}Cl$ (v = 0) recorded via the (a) $f^3\Delta_2 - X^1\Sigma^+$ (0, 0) and (b) $F^1\Delta_2 - X^1\Sigma^+$ (0,0) intermediate transitions. The background subtracted signal is shown following IR excitation at 3550 cm^{-1}.

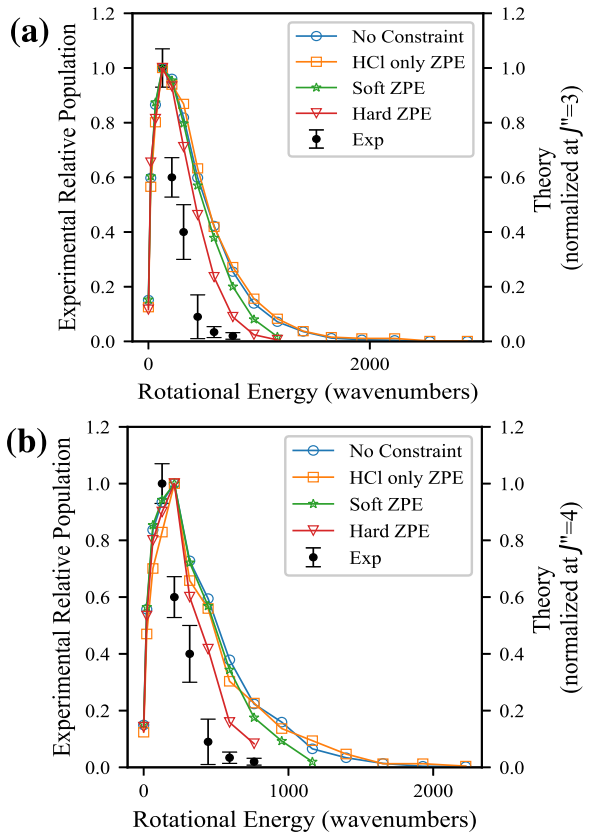

FIG. 5. Comparison between experimental (black) and QCT (indicated colors) rotational populations for the HCl fragment following dissociation of HWWW. The discrete rotational energy data points for each constraint in the calculations are connected by a line for visual guidance. Experimental REMPI intensities were converted to relative populations using published correction factors.[27,28] REMPI data obtained using different intermediate states were used and the populations were normalized to $J'' = 5$ for which transitions to all intermediate states were recorded. The QCT calculations are for excitation of (a) mode 22 and (b) mode 24 and were normalized by the maximum populations, $J'' = 3$ and 4, respectively.

and the experimental inability to detect reliably rotational levels greater than $J'' = 8$ above the background. Overall, we consider the agreement between theory and experiment satisfactory.

The QCT rotational energy distributions (corresponding to excitation of mode 24) for the water fragment in Pathway 2 are shown in Fig. 6(b). With the theoretically calculated D_0, the maximum rotational energy should be 724 cm^{-1} by conservation of energy; as seen, this maximum is observed for the soft and hard ZPE constraints on both products. The corresponding plots for excitation of mode 22, shown in Fig. 6(a), are very similar to the ones shown in Fig. 6(b).

Experimentally, the H_2O 2+1 REMPI spectrum recorded via the $\tilde{C}^1B_1(000)$ state is too congested to obtain a detailed H_2O rotational state distribution. However, the spectrum reported in Fig. 2 of Ref. 17 could be fit fairly well with a temperature of 300 K for transitions originating from higher rotational levels (for example, $J''_{Ka,Kc} = 5_{0,5}$ and $7_{0,7}$) by using the PGOPHER simulation [Fig. 7(b)].[24] On the other hand, transitions from the lower rotational levels, such as $J''_{Ka,Kc}$ = $2_{2,1}$ and $3_{2,1}$, clearly fit better with a lower temperature of ~150 K [Fig. 7(a)]. The corresponding average rotational

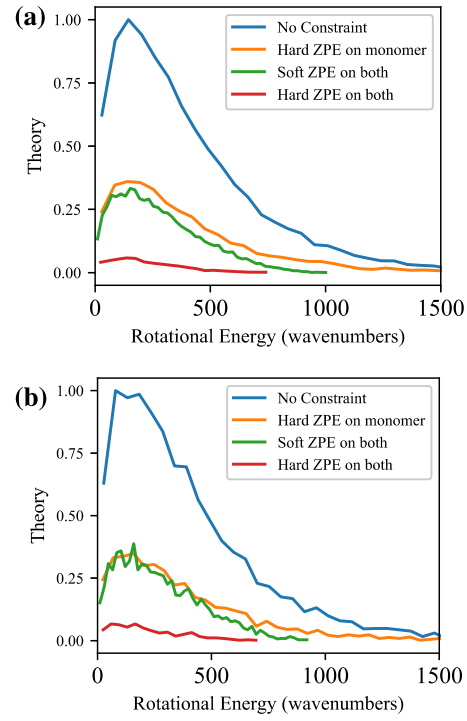

FIG. 6. QCT water monomer rotational energy distributions for Pathway 2 calculated using the indicated constraints for 3550 cm^{-1} excitation of (a) mode 22 and (b) mode 24.

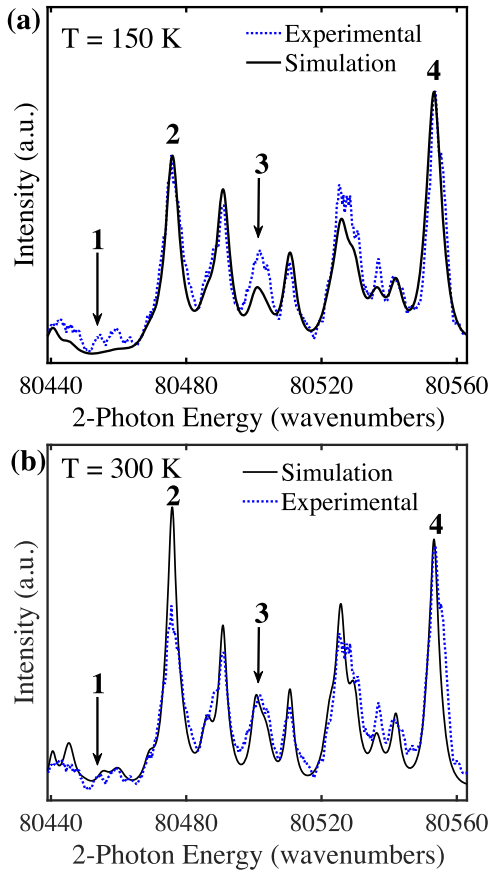

FIG. 7. Background subtracted 2 + 1 REMPI spectra (blue) and simulation of the spectra (black) at (a) T = 150 K and (b) T = 300 K. Labeled transitions originate from $J''_{Ka,Kc}$ rotations: (1) $7_{1,6}$, (2) $3_{2,1}$, (3) $5_{0,5}/5_{1,5}$, and (4) $2_{2,1}$.

energies are about 200 and 100 cm^{-1}. It must be born in mind, however, that the predissociation factors that are included in the PGOPHER[29] fit are less accurate for high rotational levels of the $\tilde{C}^1B_1(000)$ state which may affect the fit.[24,34] Another possible reason for the higher temperature corresponding to the higher rotational levels is contributions from hot bands, as discussed above. Boltzmann plots of the calculated distributions (shown in Fig. S4 of the supplementary material) are fit well (at low rotational energies) with temperatures of 327, 306, 205, and 160 K for no constraint, a hard constraint on the water monomer, soft constraints on both ZPEs, and hard constraints on both ZPEs, respectively. It appears, therefore, that the rotational distribution of the water fragment is statistical-like and can be described within the temperature range of 150–300 K (rotational energies of 100–200 cm^{-1}).

C. Dissociative trajectories and lifetimes

Examination of dissociative trajectories can shed light on mechanisms; snapshots from two representative trajectories are shown in Fig. 8. As stated above, the calculated dissociation energies for both pathways correspond to cyclic trimer fragments. Indeed, it is evident from Fig. 8 that just prior to dissociation, the polyatomic fragments form cyclic structures, sometimes with the monomer fragment still attached to the trimer ring by a H-bond. In fact, the product water trimer ring breaks and reforms many times during the dissociation until the monomer (HCl or H_2O) eventually separates, and there are many intermediate structures seen in each trajectory. No low-energy open-chain stable trimer fragments were found in the calculations, and we conclude that the VP products are a monomer and a cyclic fragment. The fragments may evolve via intermediates that have the monomer H-bonded to the cyclic trimer, as seen, for example, in the HCl trajectory in Fig. 8(a). The multiple break-up and formation of H-bonds appear to be a common motif in the VP of small clusters. In our work, we have seen them in trajectories of VP of $(H_2O)_2$, $(H_2O)_3$, and $(HCl)_3$.[1,20–22]

The calculated vibrational predissociation lifetimes for HWWW are similar for excitation of modes 22 and 24 and are significantly shorter than those of smaller cluster systems. Both pathways show lifetimes of about 8 ps, compared to the water trimer (84% dissociated at 10.5 ps) and the water dimer (84% dissociated at 25 ps).[1,20] The linewidths in the vibrational spectrum of HWWW obtained in He droplets are of the order of 3–6 cm^{-1}.[16] While the He droplet environment may cause some broadening, the observed linewidths, which correspond to lifetimes of several picoseconds, are in agreement with the results of the trajectory calculations.

Based solely on the cluster size, the trend is that larger clusters have shorter dissociation lifetimes. This trend may be explained partly by the time it takes for the initial OH stretch excitation to couple to low-energy intermolecular vibrational levels of the cluster. For example, the lifetime of the H_2O trimer is much shorter than that of the HCl trimer, because of the existence of a bending mode in the water monomer, which facilitates coupling to the intermolecular modes in the latter.[1,21,22] The lifetime of >1 ns for the HCl trimer is indeed correlated with the persistence of its coupled HCl stretch modes.[22] In the present work, the excited H-bonded OH stretch of the tetramer is likely to couple more efficiently to the intermolecular modes than in the water trimer because of the higher density of states of intermolecular modes in the tetramer. Also, the nominal OH stretch vibrations have contributions from other motions, which may facilitate coupling. Therefore, it is reasonable that the lifetimes of larger clusters become shorter although at some point the statistical nature of the predissociation process will cause the rates to decrease with cluster size. In large clusters, we expect that energy disposition would be more statistical-like, although because of the relatively large energy separation between the rotational levels of the HCl monomer, some deviations from statistical behavior would not be surprising. Strong evidence for statistical behavior comes from the similarities in final state distributions from the QCT calculations exciting either OH stretch mode 22 or 24. Overall, the VP of HWWW observed in our work is typical of that of other cyclic clusters, such as $(HCl)_3$ and $(H_2O)_3$. However, as noted above, in this study, we experimentally probe only neutral H_2O and HCl fragments; therefore, we are unable to see either ionization to H_3O^+ and Cl^- or zwitterionic behavior. Fárník *et al.* raised the possibility of the latter and speculated

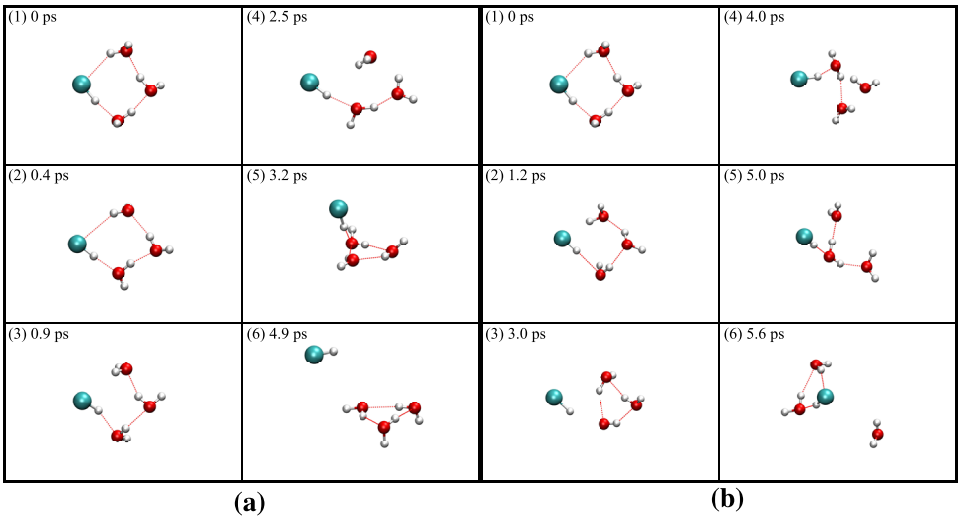

FIG. 8. (a) Trajectory snapshots of Pathway 1 for (~6 ps) and (b) Pathway 2 for (~7 ps) following excitation of mode 22.

that it might be evidenced in their IR spectrum of the mixed clusters by the observation of a "broad hump" (~150 cm^{-1}) at 2180 cm^{-1}.[35]

The branching ratio for the two pathways can be obtained from the QCT calculations; however, the results are very sensitive to the ZPE constraint used, as expected. With no ZPE constraint, the branching ratio for Pathway 1 to 2 is 0.77 to 1, with the soft ZPE constraint it is 0.99 to 1, and with the hard ZPE constraints it is 1.76 to 1. With the hard ZPE constraints and using the calculated values of D_0 for the two pathways, the excess energy for Pathway 1 is 1124 cm^{-1} (3550–2426 cm^{-1}) and for Pathway 2 it is 724 cm^{-1} (3550–2826 cm^{-1})—a difference of roughly 400 cm^{-1}. However, for the PES the difference is 500 cm^{-1}, owing to the differences in the PES D_e and the CBS values. In any case, the difference in energy certainly favors Pathway 1 over Pathway 2. However, without the ZPE constraint, Pathway 2 is slightly favored even though the difference in electronic energies is even larger, namely, 600 cm^{-1} from the CBS values and 700 cm^{-1} from the PES values. Naively, there are three ways to eliminate a water monomer and only one way to eliminate HCl, which would lead to a branching ratio of 0.33 to 1 if the two channels were isoenergenic. This ratio is not observed, even without any ZPE constraint, suggesting that the branching ratio is not a simple statistical one. Unfortunately, because of the different experimental conditions used in optimizing signals from the two VP pathways, the branching ratio cannot be obtained experimentally.

V. SUMMARY AND CONCLUSIONS

The VP of cyclic HWWW, the largest HCl–$(H_2O)_n$ cluster that is not ionized to $H_3O^+ + Cl^-$, has been investigated by both theory and experiment. The cluster was excited experimentally at 3550 cm^{-1} corresponding to an H-bonded OH stretch fundamental. QCT calculations considered excitation of each of the two H-bonded OH stretch fundamentals closest in energy to the one excited in the experiment. The results for the two modes were very similar. HCl and H_2O have been identified as the products of Pathways 1 and 2, respectively. Calculations show that these pathways terminate in the corresponding cyclic trimer products and their D_0 values are 2426 ± 23 cm^{-1} and 2826 ± 19 cm^{-1}, respectively. The corresponding experimental values, estimated from the endpoints of the fragments' speed distributions, are lower but in the same order: 2100 ± 300 cm^{-1} and 2400 ± 100 cm^{-1}. Arguments are presented that the most likely reason for the discrepancy is contributions from hot bands of the clusters, which contribute mainly to the high-speed tails.

The shapes of the HCl pair-correlated speed distributions, their peaks and averages, and the average c.m. translational energies all show better agreement between theory and experiment, with small deviations attributed mainly to the high-speed tails. Likewise, the rotational energy distributions of the HCl and H_2O monomer fragments show satisfactory agreement between theory and experiment.

Trajectory calculations show that the dissociation lifetime is of the order of 10 ps, and during each trajectory, terminating in either HCl or H_2O monomer fragments, H-bonds are broken and reformed many times, until the monomer detaches completely leaving a cyclic trimer as the cofragment. Such behavior is typical in the VP of other small clusters of HCl and/or H_2O, where the rate limiting step is often the initial coupling of the excited OH or HCl stretch vibration to other intramolecular and intermolecular vibrations of the cluster, followed by energy randomization in the excited cluster and finally dissociation.

Except for the branching ratios of Pathways 1 and 2, which are calculated to be nonstatistical, energy partitioning in the other degrees of freedom appear statistical-like, as is typical of clusters with a high density of vibrational states. Overall, the VP of HWWW is typical of that of other clusters of comparable size.

SUPPLEMENTARY MATERIAL

See supplementary material for the experimental beam temperature and HCl rotational state populations, normal mode analysis (NMA) of the parent cluster, calculated dissociation energies, comparison between experimental and varied ZPE constraint calculations, and estimated water fragment temperatures calculated using different ZPE constraints. Some comparisons of QCT results obtained for excitation of modes 22 and 24 are also given.

ACKNOWLEDGMENTS

We thank Mitchell Butler for his dedicated assistance in data acquisition and analysis and John Mancini for his calculations of the dissociation energies for the pathways. We also thank the reviewers for very helpful comments. This work is supported by the National Science Foundation Grant Nos. CHE-1664994 (H.R.) and CHE-1463552 (J.M.B.).

[1] A. K. Samanta, Y. Wang, J. S. Mancini, J. M. Bowman, and H. Reisler, Chem. Rev. **116**, 4913 (2016).
[2] S. Scheiner, *Noncovalent Forces* (Springer, 2015).
[3] V. E. Bondybey, M. Beyer, U. Achatz, S. Joos, and G. Niedner-Schatteburg, Isr. J. Chem. **39**, 213 (1999).
[4] M. Masia, H. Forbert, and D. Marx, J. Phys. Chem. A **111**, 12181 (2007).
[5] H. Forbert, M. Masia, A. Kaczmarek-Kedziera, N. N. Nair, and D. Marx, J. Am. Chem. Soc. **133**, 4062 (2011).
[6] K. Andot and J. T. Hynes, J. Mol. Liq. **64**, 25–37 (1995).
[7] S. Sugawara, T. Yoshikawa, T. Takayanagi, and M. Tachikawa, Chem. Phys. Lett. **501**, 238 (2011).
[8] G. M. Chaban, R. B. Gerber, and K. C. Janda, J. Phys. Chem. A **105**, 8323 (2001).
[9] J. S. Mancini and J. M. Bowman, Phys. Chem. Chem. Phys. **17**, 6222 (2015).
[10] A. Vargas-Caamal, J. L. Cabellos, F. Ortiz-Chi, H. S. Rzepa, A. Restrepo, and G. Merino, Chem. - Eur. J **22**, 2812 (2016).
[11] N. Guggemos, P. Slavíček, and V. V. Kresin, Phys. Rev. Lett. **114**, 043401 (2015).
[12] M. J. Packer and D. C. Clary, J. Phys. Chem. **99**, 14323 (1995).
[13] D. E. Bacelo, R. C. Binning, Jr., and Y. Ishikawa, J. Phys. Chem. A **103**, 4631 (1999).
[14] J. S. Mancini and J. M. Bowman, J. Phys. Chem. Lett. **5**, 2247 (2014).
[15] S. Odde, B. J. Mhin, S. Lee, H. M. Lee, and K. S. Kim, J. Chem. Phys. **120**, 9524 (2004).
[16] J. Zischang, D. Skvortsov, M. Y. Choi, R. A. Mata, M. A. Suhm, and A. F. Vilesov, J. Phys. Chem. A **119**, 2636 (2015).
[17] K. Zuraski, D. Kwasniewski, A. K. Samanta, and H. Reisler, J. Phys. Chem. Lett. **7**, 4243 (2016).
[18] A. K. Samanta, G. Czakó, Y. Wang, J. S. Mancini, J. M. Bowman, and H. Reisler, Acc. Chem. Res. **47**, 2700 (2014).

[19]B. E. Rocher-Casterline, A. K. Mollner, L. C. Ch'ng, and H. Reisler, J. Phys. Chem. A **115**, 6903 (2011).
[20]L. C. Ch'ng, A. K. Samanta, G. Czakó, J. M. Bowman, and H. Reisler, J. Am. Chem. Soc. **134**, 15430 (2012).
[21]L. C. Ch'ng, A. K. Samanta, Y. Wang, J. M. Bowman, and H. Reisler, J. Phys. Chem. A **117**, 7207 (2013).
[22]J. S. Mancini, A. K. Samanta, J. M. Bowman, and H. Reisler, J. Phys. Chem. A **118**, 8402 (2014).
[23]D. S. Green, G. A. Bickel, and S. C. Wallace, J. Mol. Spec. **150**, 388 (1991).
[24]C.-H. Yang, G. Sarma, J. J. ter Meulen, D. H. Parker, and C. M. Western, Phys. Chem. Chem. Phys. **12**, 13983 (2010).
[25]V. Dribinski, A. Ossadtchi, V. A. Mandelshtam, and H. Reisler, Rev. Sci. Instrum. **73**, 2634 (2002).
[26]J. Mooney and P. Kambhampati, J. Phys. Chem. Lett. **4**, 3316 (2013).
[27]M. Korolik, D. W. Arnold, M. J. Johnson, M. M. Suchan, H. Reisler, and C. Wittig, Chem. Phys. Lett. **284**, 164 (1998).
[28]S. Rudić, D. Ascenzi, and A. Orr-Ewing, J. Chem. Phys. Lett. **332**, 487 (2000).
[29]C. M. Western, PGOPHER, a program for simulating rotational, vibrational, and electronic spectra, University of Bristol, Bristol, UK, http://pgopher.chm.bris.ac.uk.
[30]T. Beyer and D. F. Swinehart, Commun. ACM **16**, 379 (1973).
[31]T. Baer and W. L. Hase, *Unimolecular Reaction Dynamics: Theory and Experiments* (Oxford University Press, Inc., New York, 1996).
[32]F. N. Keutsch, J. D. Cruzan, and R. J. Saykally, Chem. Rev. **103**, 2533 (2003).
[33]A. K. Mollner, B. E. Casterline, L. C. Ch'ng, and H. Reisler, J. Phys. Chem. A **113**, 10174 (2009).
[34]C. M. Western, private communication (2017).
[35]M. Fárník, M. Weimann, and M. A. Suhm, J. Chem. Phys. **118**, 10120 (2003).